

ATTITUDE CONTROL ALGORITHMS IN A SWARM OF CUBESATS: KRIGING INTERPOLATION AND COORDINATED DATA EXCHANGE

Anton Afanasev*, Anton Ivanov†, Ahmed Mahfouz‡, and Dmitry Pritykin§

This study is a part of the Skoltech University project to deploy a swarm of four identical 3U CubeSats in LEO. The CubeSats are to be equipped with gamma-ray sensors and their collective behavior will be exhibited in detecting gamma-ray bursts and coordinated attitude control. We consider a fully magnetic attitude control system, comprising a magnetometer as a part of attitude determination routine and three orthogonal magnetorquers as actuators. Having implemented and tested the conventional three-axis magnetic attitude determination and control algorithms, we proceed to study how the performance of such ADCS may be enhanced by using measurements and state vectors exchange. We interpolate the exchanged data, using the Kriging algorithm in conjunction with Extended Kalman filter and Lyapunov-based controller, since it provides the auto-correlation and variance information about the environment of the magnetic field, which is of utmost importance for heterogeneous and noisy fields. In our simulations we compare the performance of the controller for a single satellite to that of the satellite in the swarm of CubeSats, which maintains the form of a regular tetrahedron and carries out distributed measurements with interpolation. Improved attitude stabilization for the latter scenario is demonstrated by mean squared errors.

INTRODUCTION

Distributed space systems use multi-spacecraft formations to replace large single-satellite architectures with the aim of enhancing mission reliability and achievable outcomes while lowering costs.¹ Although single-satellite missions still have advantages in terms of accuracy and functionality, new distributed architectures provide improved flexibility and adaptability to structural and functional changes.² This development is not entirely unexpected and has been foretold – among others – by Stanisław Lem,³ whose book “*Summa Technologiae*” indicates a certain similarity between biological and technological evolution, which has a tendency towards extinction of uncooperative gigantic species (whether it be dinosaurs in biology or zeppelins in technology), whereas the smaller ones go on and continue their development. One of the reasons behind this might be that the surviving smaller species are able to form large groups, communicating with each other and finding optimal ways to resolve vital issues, such as where to find food, how to attack foes etc.

*PhD student, Space Center, Skolkovo Institute of Science and Technology, Bolshoy Boulevard 30, bld. 1, Moscow, Russia 121205.

†Director, Space Center, Skolkovo Institute of Science and Technology, Bolshoy Boulevard 30, bld. 1, Moscow, Russia 121205.

‡MSc student, Space Center, Skolkovo Institute of Science and Technology, Bolshoy Boulevard 30, bld. 1, Moscow, Russia 121205.

§Senior Researcher, Space Center, Skolkovo Institute of Science and Technology, Bolshoy Boulevard 30, bld. 1, Moscow, Russia 121205.

The analogy can be extended to CubeSats swarms, which are becoming feasible, but require the adoption of new operation paradigms that, on one hand, enhance their autonomy, but on the other hand, make full use of it. Deployment of the miniature satellites' swarms promises to be fast and inexpensive. These Swarms can comprise simplistic units that detect certain events and exchange signals with each other and even larger more complicated spacecraft that acts as an analysis hub. Finally, swarms or constellations can be employed as distributed artificial intelligence. They can exhibit collective behaviour, such as self-organization, transformability, self-learning and simultaneous sensing over large areas. We shall refer the reader to an exhaustive survey by Farrag⁴ of swarm missions, which, for the moment, is mostly the technology demonstration. Among those missions that are currently planned to be deployed, we may mention the HERMES (High Energy Rapid Modular Ensemble of Satellites), which is a mission concept, based on a swarm of nano-satellites in low Earth orbit (LEO), hosting simple but fast scintillators to probe the X-ray emission of bright high-energy transients.⁵ The swarm mission, our study stems from, is also conceptually a scientific project that is currently under development at Skoltech, aiming to deploy a swarm of four identical 3U CubeSats in a LEO. The CubeSats are to carry gamma-ray sensors, and their collective behavior will be exhibited in detecting gamma-ray bursts and in coordinated attitude control. The CubeSats are not supposed to be equipped with propulsion systems, and the only means of controlling their dynamics to exhibit the swarm behavior is in using the attitude determination and control subsystem (ADCS). A number of studies have already been carried out with the aim of designing the spacecraft themselves and their ADCS in particular.^{6,7}

This paper addresses the problem of collective data processing and usage in a swarm of CubeSats. It namely focuses on the spacecraft's attitude determination and control subsystems (ADCS), which benefits from the distributed measurement data exchange through the intersatellite link. By processing the exchanged measurement data, the swarm is shown to recover the actual magnetic field in the areas where the swarm satellites are present. Our preliminary study⁸ has shown that even the simplest interpolation algorithm enhances the on-board magnetic field model, thus making the attitude determination algorithms more robust and more immune, for instance, to magnetic storms. To further demonstrate this effect, we consider advanced interpolation techniques that capture the spatial statistical properties of the geomagnetic field and apply them in the control loop of a fully magnetic attitude control system. We use state-of-the-art attitude control algorithms,^{9,10} which are fairly often implemented in CubeSats, because of low cost of the required hardware. We shall note, however, that the use of the proposed data exchange scheme is in no way limited to magnetic control systems and can be generalized to be employed in the attitude or even orbit determination loop in groups of satellites of various design.

The paper has the following structure. In the first sections we introduce our implementation of a fully magnetic ADCS for a single satellite.⁹ This part comprises introduction of the used reference frames, equations of motion, controller and the Extended Kalman Filter to process the magnetometer data. We then present simulation results for the single satellite scenario and quantify them using Mean-Squared Errors (MSE) metrics. Having done that, we proceed to the core part of the study devoted to the interpolation of the magnetic field measurements by the swarm of 4 CubeSats with the Kriging algorithm. Measurements optimization explicitly leads to the enhancement of the attitude control in each individual CubeSat, showing better MSEs as compared to a single satellite setup. The article ends with Conclusions, which discusses the obtained results and outlines prospective directions of future research.

REFERENCE FRAMES

Let us denote by O_{\oplus} and O_{S} the center of the Earth and a satellite's center of mass, respectively. The following reference frames will be used:

- \mathcal{F}^u Orbital reference frame $O_{\oplus}xyz$ (fig. 1a). This frame is defined by the spacecraft's argument of latitude u on the given circular orbit. z -axis extends through the current position of the satellite. y -axis direction coincides with that of the satellite's center of mass angular momentum. x -axis completes the frame to a right-handed triad (for circular orbits the x -axis runs parallel to the spacecraft's linear velocity vector). All vectors represented in this frame are denoted by the upper index u : \mathbf{v}^u (single satellite scenario).
- \mathcal{F}^q Body-fixed reference frame $O_{\text{S}}XYZ$ (fig. 1b). The three axes of this frame coincide with the spacecraft's principal axes of inertia. Usually, the smallest and the greatest moments of inertia are related to Z and Y -axis, respectively – to fulfil the gravity-gradient orientation stability conditions. The frame is obtained from the orbital frame \mathcal{F}^u by spacecraft's unit quaternion Q^* rotation. All vectors represented in this frame are denoted by the upper index q : \mathbf{v}^q (single satellite scenario).

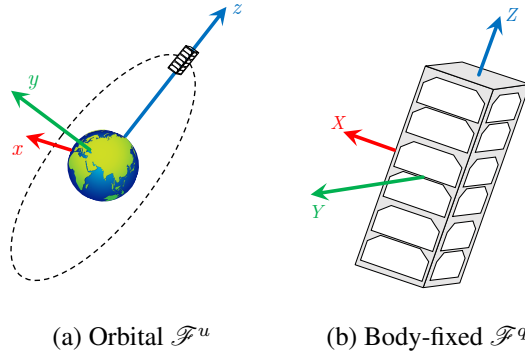


Figure 1: Reference frames.

The frames \mathcal{F}^u and \mathcal{F}^q , whose origin is fixed in the satellite, are constantly changing with respect to the center of Earth. Moreover, for the swarm scenario there will be multiple of such frames. In that case we shall enumerate them according to the number of satellites in the swarm. For interpolation purposes we shall also introduce an orbital reference frame related to the swarm's center of mass:

- \mathcal{F}_j^u Orbital reference frame of the j^{th} satellite in the swarm. All vectors represented in this frame are denoted by the upper index u_j : \mathbf{v}^{u_j} (swarm scenario).
- \mathcal{F}_0^u Orbital reference frame of the swarm's center of mass. All vectors represented in this frame are denoted by the upper index u_0 : \mathbf{v}^{u_0} (swarm scenario).
- \mathcal{F}_j^q Body-fixed reference frame of the j^{th} satellite in the swarm. All vectors represented in this frame are denoted by the upper index q_j : \mathbf{v}^{q_j} (swarm scenario).

SPACECRAFT EQUATIONS OF MOTION

Quaternion Kinematics

The unit quaternion $Q = (q_0, \mathbf{q})$ relates the spacecraft's body-frame \mathcal{F}^q to the orbital frame \mathcal{F}^u . Thus representations of any vector \mathbf{r} in these two frames \mathbf{r}^q and \mathbf{r}^u are related by

$$\mathbf{r}^u = Q \circ \mathbf{r}^q \circ Q^*,$$

where $Q^* = (q_0, -\mathbf{q})$ is the conjugate of Q .

Let $\boldsymbol{\omega}^q$ and $\boldsymbol{\Omega}^q$ denote the absolute and relative angular velocities of the spacecraft. Absolute angular velocity $\boldsymbol{\omega}^q$ then may be expressed as

$$\boldsymbol{\omega}^q = \boldsymbol{\Omega}^q + Q^* \circ \boldsymbol{\omega}_0^u \circ Q, \quad (1)$$

where $\boldsymbol{\omega}_0^u = (0 \ \omega_0 \ 0)^\top$ is the angular velocity of the orbital frame corresponding to the mean motion.

The quaternion kinematics equation for the relative motion is

$$\dot{Q} = \frac{1}{2}Q \circ \boldsymbol{\Omega}^q. \quad (2)$$

Rigid Body Dynamics

Each spacecraft is modeled as a rigid body, whose rotation is described by the Euler equations:

$$\mathbf{J}\dot{\boldsymbol{\omega}}^q + \boldsymbol{\omega}^q \times \mathbf{J}\boldsymbol{\omega}^q = \mathbf{T}^q \quad (3)$$

where \mathbf{J} is the inertia tensor of the spacecraft, \mathbf{T}^q is the resultant torque acting upon the body. The resultant torque is given by:

$$\mathbf{T}^q = \mathbf{T}_{\text{ctrl}}^q + \mathbf{T}_{\text{grav}}^q + \mathbf{T}_{\text{dist}}^q, \quad (4)$$

where $\mathbf{T}_{\text{ctrl}}^q$ is the control torque, $\mathbf{T}_{\text{grav}}^q$ is the gravity-gradient torque, and $\mathbf{T}_{\text{dist}}^q$ is the disturbance torque.

The control torque $\mathbf{T}_{\text{ctrl}}^q$ is modeled as

$$\mathbf{T}_{\text{ctrl}}^q = \mathbf{m}^q \times \overline{\mathbf{B}}^q, \quad (5)$$

where $\overline{\mathbf{B}}^q$ is true value of the geomagnetic field, \mathbf{m}^q is the magnetic moment generated by three mutually orthogonal magnetorquers that each spacecraft is equipped with. The algorithm, according to which the magnetic moment is generated, is described in the next section.

The gravity-gradient torque $\mathbf{T}_{\text{grav}}^q$ is given by:

$$\mathbf{T}_{\text{grav}}^q = 3\omega_0^2 \mathbf{e}_Z^q \times \mathbf{J}\mathbf{e}_Z^q \quad (6)$$

where $\mathbf{e}_Z^q = Q^* \circ \mathbf{e}_z^u \circ Q = Q^* \circ (0 \ 0 \ 1)^\top \circ Q$ is the unit vector of Z -axis in \mathcal{F}^q , which is quaternion-rotated ort of z -axis in \mathcal{F}^u .

Disturbance torque $\mathbf{T}_{\text{dist}}^q$ comprises all explicitly unaccounted for external torques (i.e. torques due to atmospheric drag, solar radiation pressure, and residual magnetization) and all sorts of internal noise processes, which may also generate parasitic torques. In this study the disturbance torque is modeled as a normally distributed random variable with mean value of some static torque $\mathbf{T}_{\text{stat}}^q$ and standard deviation σ_{torque} with corresponding covariance matrix $\boldsymbol{\Sigma}_{\text{torque}} = \sigma_{\text{torque}}^2 \mathbf{I}$, where \mathbf{I} is the identity matrix:

$$\mathbf{T}_{\text{dist}}^q = \boldsymbol{\eta}_{\text{torque}} \sim \mathcal{N}(\mathbf{T}_{\text{stat}}^q, \boldsymbol{\Sigma}_{\text{torque}}) \quad (7)$$

CONTROL MAGNETIC MOMENT

The magnetic moment is computed with the aid of the well-known PD algorithm⁹

$$\mathbf{m}^q = k_\omega \Delta \boldsymbol{\Omega}^q \times \mathbf{B}^q + k_s \mathbf{S}^q \times \mathbf{B}^q, \quad (8)$$

where $\Delta \boldsymbol{\Omega}^q = \boldsymbol{\Omega}^q - \boldsymbol{\Omega}_{\text{des}}^q$ is the angular velocity error, $\mathbf{S}^q = 4q_0 \mathbf{q}$ is the attitude error corresponding to the error quaternion Q , \mathbf{B}^q is the on-board estimate of the external geomagnetic field, k_ω and k_s are the control gains.

In this study the required attitude is attained when the orbital and the body-frame coincide, which means that the required attitude corresponds to the identity quaternion and the required relative angular velocity is zero.

Coefficients k_ω and k_s are tuned via Floquet theory. The basic procedure¹¹ is to minimize the maximal eigenvalue of the monodromy matrix, constituted of the values of motion equations' fundamental matrix of solutions after spacecraft's one revolution on the orbit.

Equations (2) and (8) in the linear approximation and assuming that the geomagnetic field is modeled as the direct dipole form a system with periodic coefficients (as required by the Floquet theory):

$$\frac{d}{du} \begin{pmatrix} \boldsymbol{\Omega}^q \\ \mathbf{S}^q \end{pmatrix} = \mathcal{J} \begin{pmatrix} \boldsymbol{\Omega}^q \\ \mathbf{S}^q \end{pmatrix}, \quad (9)$$

where the Jacobian matrix \mathcal{J} is given by

$$\mathcal{J} = \frac{\partial \begin{pmatrix} \frac{d\boldsymbol{\Omega}^q}{du} & \frac{d\mathbf{S}^q}{du} \end{pmatrix}}{\partial \begin{pmatrix} \boldsymbol{\Omega}^q & \mathbf{S}^q \end{pmatrix}} \quad (10)$$

Let \mathcal{X} be the fundamental matrix of solutions to the system of equations (9). Since \mathcal{J} is periodic with respect to the argument of latitude u : $\mathcal{J}(u + T_u) = \mathcal{J}(u)$ with $T_u = 2\pi$, and initial condition for the fundamental matrix \mathcal{X} is $\mathcal{X}(0) = \mathbf{I}$, the following relation holds

$$\mathcal{X}(u + T_u) = \mathcal{X}(u)\mathcal{X}(T_u), \quad (11)$$

where $\mathcal{X}(T_u)$ is the monodromy matrix for the fundamental matrix \mathcal{X} and will be denoted as \mathcal{M} .

Finally, the monodromy matrix $\mathcal{M} = \mathcal{X}(2\pi)$ is obtained from the following ODE, solved for the time-span of exactly one period $u \in [0, 2\pi]$

$$\begin{aligned} \frac{d\mathcal{X}}{du} &= \mathcal{J}\mathcal{X}, \\ \mathcal{X}(0) &= \mathbf{I}. \end{aligned} \quad (12)$$

The values for control gains k_ω and k_s are then obtained as:

$$k_\omega^*, k_s^* = \arg \min_{k_\omega, k_s} \max_j \Re(\ln \lambda_j), \quad (13)$$

where $\lambda_j = \lambda_j(k_\omega, k_s)$ are eigenvalues of the monodromy matrix \mathcal{M} .

The outlined procedure is illustrated by figure 2, which shows the contour plot of $\max_j \Re \ln \lambda_j$ as a function of the two gains' values ($k_\omega' = k_\omega \omega_0$). It is worth noting that a sufficient condition for controller convergence from Eq. (8) requires $\max_j \Re \ln \lambda_j$ to be strictly negative.

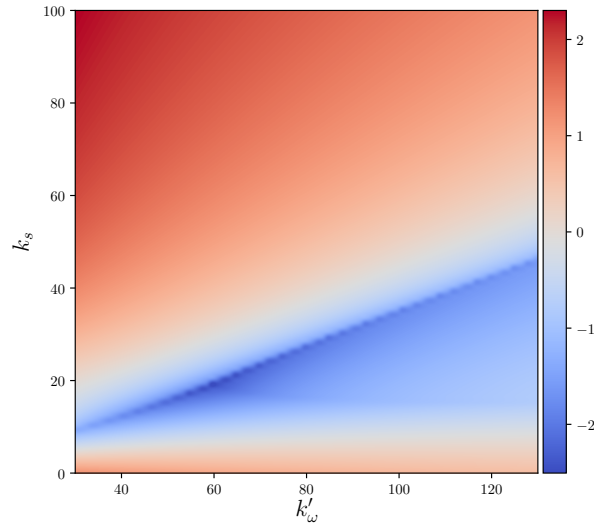


Figure 2: Stability area for CubeSat with inertia tensor $\mathbf{J} = \text{diag}(0.011, 0.014, 0.009)$ [$\text{kg} \cdot \text{m}^2$] on a circular orbit with altitude $h_{\text{orb}} = 750$ km and inclination $i = 60^\circ$.

GEOMAGNETIC FIELD

In order to preserve the periodicity of Jacobian \mathcal{J} from Eq. (9) the direct dipole model of the geomagnetic field is used throughout the paper as a baseline model. The direct dipole can be expressed in the orbital reference frame as¹¹

$$\mathbf{B}^u = \frac{\mu_e \mu_0}{4\pi R^3} \begin{pmatrix} \cos u \sin i \\ \cos i \\ -2 \sin u \sin i \end{pmatrix}, \quad (14)$$

where \mathbf{R} is the position vector of a point in space having absolute value R , $\mu_e = 7.94 \cdot 10^{22}$ A \cdot m² is the Earth magnetic dipole moment, $\mu_0 = 1.257 \cdot 10^{-6} \frac{\text{N}}{\text{A}^2}$ is the vacuum permeability, u and i are the argument of latitude and orbit inclination, respectively.

The magnetic field is measured by the spacecraft's on-board magnetometer. Measurement errors are modeled as normal distribution with mean value of magnetometer bias $\mathbf{B}_{\text{bias}}^q$ and standard deviation σ_{meas} with corresponding covariance matrix $\Sigma_{\text{meas}} = \sigma_{\text{meas}}^2 \mathbf{I}$:

$$\boldsymbol{\eta}_{\text{meas}} \sim \mathcal{N}(\mathbf{B}_{\text{bias}}^q, \Sigma_{\text{meas}}). \quad (15)$$

Thus, the measurement model is given by:

$$\tilde{\mathbf{B}}^q = \mathbf{Q}^* \circ \mathbf{B}^u \circ \mathbf{Q} + \boldsymbol{\eta}_{\text{meas}}. \quad (16)$$

where $\tilde{\mathbf{B}}^q$ is the measurement of the magnetometer in the body-fixed frame \mathcal{F}^q .

The same direct dipole model with the environmental noise $\boldsymbol{\eta}_{\text{env}}$ introduced to model the actual magnetic field surrounding the spacecraft. The noise has normal distribution with zero mean and covariance matrix $\Sigma_{\text{env}} = \sigma_{\text{env}}^2 \mathbf{I}$:

$$\boldsymbol{\eta}_{\text{env}} \sim \mathcal{N}(\mathbf{0}, \Sigma_{\text{env}}). \quad (17)$$

Finally, the environmental model is:

$$\bar{\mathbf{B}}^q = Q^* \circ \mathbf{B}^u \circ Q + \boldsymbol{\eta}_{\text{env}}, \quad (18)$$

where $\bar{\mathbf{B}}^q$ is the true value of the magnetic field in the measurement point in \mathcal{F}^q .

EXTENDED KALMAN FILTER

The Kalman filter represents recursive estimation of the state vector $\mathbf{X}(t)$ of an a priori known dynamical system.¹² To calculate the current i^{th} state of the system $\mathbf{X}_i = \mathbf{X}(t_i)$ it is necessary to obtain the current measurement $\mathbf{z}_i = \mathbf{z}(t_i)$ and know the previous state $\mathbf{X}_{i-1} = \mathbf{X}(t_{i-1})$. Unlike other recursive filters, the Kalman filter operates not only with the state estimates, but also with estimates of the uncertainty of the state vector in the form of covariance matrix $\mathbf{P}_i = \mathbf{P}(t_i)$.

As we deal with a nonlinear system the Extended Kalman Filter (EKF) will be employed. The general form of a nonlinear system for EKF is written as follows:

$$\begin{aligned} \dot{\mathbf{X}}(t) &= f(\mathbf{X}(t)) + \mathbf{G}\mathbf{w}(t) \\ \mathbf{z}_i &= h(\mathbf{X}_i) + \mathbf{v}_i \end{aligned} \quad (19)$$

where function f is the evolution of vector \mathbf{X} , function h is the measurement model of vector \mathbf{X} , \mathbf{w} and \mathbf{v} are process and observation noises, respectively, with normal distribution and covariance matrices $\boldsymbol{\Sigma}_{\mathbf{w}}$ and $\boldsymbol{\Sigma}_{\mathbf{v}}$:

$$\begin{aligned} \mathbf{w}(t) &\sim \mathcal{N}(\mathbf{E}\mathbf{w}(t), \boldsymbol{\Sigma}_{\mathbf{w}}(t)) \\ \mathbf{v}_i &\sim \mathcal{N}(\mathbf{E}\mathbf{v}_i, \boldsymbol{\Sigma}_{\mathbf{v}i}) \end{aligned} \quad (20)$$

where \mathbf{E} – expected value; and \mathbf{G} is the matrix of the process noise \mathbf{w} influence on the state-space vector \mathbf{X} .

Let $\tilde{\mathbf{X}}$ and $\hat{\mathbf{X}}$ denote the predicted (or extrapolated) and corrected (or filtered) estimates of the state-space vector, respectively, and let $\tilde{\mathbf{P}}$ and $\hat{\mathbf{P}}$ be the corresponding covariance matrices. The predicted value of the vector is obtained out of the corrected one in the previous time step via the evolution function f from (19):

$$\begin{aligned} \dot{\mathbf{X}}(t) &= f(\mathbf{X}(t)) \\ \text{w.r.t. } \mathbf{X}(t_{i-1}) &= \hat{\mathbf{X}}_{i-1} \implies \mathbf{X}(t_i) = \tilde{\mathbf{X}}_i \end{aligned} \quad (21)$$

Let \mathbf{F}_i and \mathbf{H}_i be evolution and observation matrices, respectively:

$$\mathbf{F}_i = \left. \frac{\partial f}{\partial \mathbf{X}} \right|_{\mathbf{X}=\hat{\mathbf{X}}_{i-1}} \quad \mathbf{H}_i = \left. \frac{\partial h}{\partial \mathbf{X}} \right|_{\mathbf{X}=\tilde{\mathbf{X}}_i} \quad (22)$$

The covariance matrix of the discrete-time process noise with respect to state-space vector is given by

$$\boldsymbol{\Sigma}_{\mathbf{G}\mathbf{w}} = \int_{t_{i-1}}^{t_i} \boldsymbol{\Phi}_i \mathbf{G} \boldsymbol{\Sigma}_{\mathbf{w}} \mathbf{G}^\top \boldsymbol{\Phi}_i^\top dt, \quad (23)$$

where $\boldsymbol{\Phi}_i$ is the transition matrix between steps $i-1$ and i :

$$\boldsymbol{\Phi}_i = \exp[\mathbf{F}_i(t_i - t_{i-1})] \quad (24)$$

Covariance matrix prediction $\tilde{\mathbf{P}}_i$ on the basis of Eqs. (24) and (23) becomes as follows:

$$\tilde{\mathbf{P}}_i = \Phi_i \hat{\mathbf{P}}_{i-1} \Phi_i^\top + \Sigma_{\mathbf{G}\mathbf{w}} \quad (25)$$

Having completed the prediction step with Equations (21) and (25) we proceed to the correction step, which is given by:

$$\begin{aligned} \mathbf{K}_i &= \tilde{\mathbf{P}}_i \mathbf{H}_i^\top \left(\mathbf{H}_i \tilde{\mathbf{P}}_i \mathbf{H}_i^\top + \Sigma_{\mathbf{v}_i} \right)^{-1} \\ \hat{\mathbf{X}}_i &= \tilde{\mathbf{X}}_i + \mathbf{K}_i \left(\mathbf{z}_i - h \left(\tilde{\mathbf{X}}_i \right) \right) \\ \hat{\mathbf{P}}_i &= (\mathbf{I} - \mathbf{K}_i \mathbf{H}_i) \tilde{\mathbf{P}}_i \end{aligned} \quad (26)$$

Satellite Attitude Control

The state-space vector for satellite attitude¹³ in the orbital reference frame \mathcal{F}^u is:

$$\mathbf{X} = \begin{pmatrix} \mathbf{q} \\ \boldsymbol{\omega}^q \end{pmatrix} \quad (27)$$

The evolution function f is given by Eq. (2) and Eq. (3). The evolution matrix \mathbf{F}_i from Eq. (22) is simplified to the constant:

$$\mathbf{F} = \begin{pmatrix} \mathbf{0}_{3 \times 3} & \frac{1}{2} \mathbf{I}_{3 \times 3} \\ \mathbf{0}_{3 \times 3} & \mathbf{0}_{3 \times 3} \end{pmatrix} \quad (28)$$

with the corresponding transition matrix from Eq. (24) (assuming constant time step):

$$\Phi = \begin{pmatrix} \mathbf{I}_{3 \times 3} & \frac{1}{2} \mathbf{I}_{3 \times 3} \cdot \Delta t \\ \mathbf{0}_{3 \times 3} & \mathbf{I}_{3 \times 3} \end{pmatrix} \quad (29)$$

where $\Delta t = t_{\text{ctrl}} + t_{\text{meas}}$ is the control loop period, which includes period of actuation t_{ctrl} (when the magnetorquers generate the control moment) and period of measurements t_{meas} (when the magnetorquers are switched off and the external magnetic field can be measured by the on-board magnetometer).

The model noise \mathbf{w} with corresponding covariance matrix $\Sigma_{\mathbf{w}}$ and matrix of influence \mathbf{G} is associated with $\mathbf{T}_{\text{dist}}^q$ from Eq. (7):

$$\mathbf{E}\mathbf{w} = \mathbf{T}_{\text{stat}}^q \quad \Sigma_{\mathbf{w}} = \sigma_{\text{torque}}^2 \mathbf{I}_{3 \times 3} \quad \mathbf{G} = \begin{pmatrix} \mathbf{0}_{3 \times 3} \\ \mathbf{J}^{-1} \end{pmatrix} \quad (30)$$

The measurement model h is obtained from Eq. (16):

$$h(\mathbf{X}) = Q^* \circ \mathbf{B}^u \circ Q \quad (31)$$

The observation matrix \mathbf{H}_i from Eq. (22) is obtained from linearized Eq. (31):

$$\mathbf{H}_i = \left(2\mathbf{W}_{h(\tilde{\mathbf{X}}_i)} \quad \mathbf{0}_{3 \times 3} \right) \quad (32)$$

where \mathbf{W}_s for vector $\mathbf{s} = (s_1 \ s_2 \ s_3)^\top$ is a skew-symmetric matrix given by:

$$\mathbf{W}_s = \begin{pmatrix} 0 & -s_3 & s_2 \\ s_3 & 0 & -s_1 \\ -s_2 & s_1 & 0 \end{pmatrix} \quad (33)$$

The observation noise \mathbf{v} with corresponding covariance matrix $\Sigma_{\mathbf{v}}$ is associated with $\boldsymbol{\eta}_{\text{meas}}$ from Eq. (15):

$$\mathbf{E}\mathbf{v} = \mathbf{B}_{\text{bias}}^q \quad \Sigma_{\mathbf{v}} = \sigma_{\text{meas}}^2 \mathbf{I}_{3 \times 3} \quad (34)$$

SINGLE SATELLITE SCENARIO

This section presents the simulations results for a single 3U CubeSat scenario. The CubeSat is assumed to be in a circular orbit (altitude $h_{\text{orb}} = 750$ km; inclination $i = 60^\circ$). The CubeSat's tensor of inertia is $\mathbf{J} = \text{diag}(0.011, 0.014, 0.009) \text{ kg} \cdot \text{m}^2$. The output of the magnetorquers is limited by $|\mathbf{m}_{\text{max}}| = 0.1 \text{ A} \cdot \text{m}^2$. The control loop time settings are $t_{\text{ctrl}} = 5$ s and $t_{\text{meas}} = 1$ s. The controller gains are tuned to $(k'_\omega, k_s) = (60, 8) \frac{\text{N} \cdot \text{m}}{\text{T}^2}$.

The result of the controlled dynamics simulation is shown in the figure 3. The plots portray the dynamics of the satellite's angular velocity and orientation expressed through the Euler angles.

Simulation Results for Perturbed Dynamics

In this section we show the results of perturbed dynamics simulation that require the Kalman filter. Let us list the settings used in the EKF algorithm.

Initial state-space vector: $\mathbf{X}_0 = \mathbf{0}_{6 \times 1}$. These values are used to initialize both the dynamical model and the Kalman filter.

Initial covariance matrix: $\mathbf{P}_0 = \text{diag}(\sigma_{q_0}^2, \sigma_{q_0}^2, \sigma_{q_0}^2, \sigma_{\omega_0}^2, \sigma_{\omega_0}^2, \sigma_{\omega_0}^2)$, where σ_{q_0} and σ_{ω_0} are assumptions of the maximum (or big enough) errors of quaternions and angular velocities respectively. In this study $\sigma_{q_0} = \frac{\pi}{2}$ and $\sigma_{\omega_0} = \frac{\pi}{18} \left[\frac{\text{rad}}{\text{s}} \right]$.

Noise parameters:
static torque $\mathbf{T}_{\text{stat}} = 0$; standard deviation of torque noise $\sigma_{\text{torque}} = 5 \text{ nN} \cdot \text{m}$; magnetometer bias $\mathbf{B}_{\text{bias}} = 0$; standard deviation of measurement noise $\sigma_{\text{meas}} = 1 \text{ nT}$; standard deviation of environmental noise $\sigma_{\text{env}} = 1 \text{ nT}$.

The result of the simulation is shown in the figure 4. In contrast to the previous figure the plots in the figure 4 zoom in to the region of smaller values of both angular velocities and Euler angles, thus giving a clear picture of the actual stabilization and pointing accuracy.

Accuracy (Mean-Squared Errors)

In order to assess the quality of the ADCS performance we run multiple simulations and gather statistics on the attitude and stabilization accuracy. The results of this numerical experiment are shown in the figure 5. The number of simulations processed is $M = 50$.

It can be seen from the plots in the figure 5 that the controller and the filter generally converge to the values of Euler angles bounded by 3.5 degrees (in all three axes), which is a reasonable enough performance for the modeled disturbances.

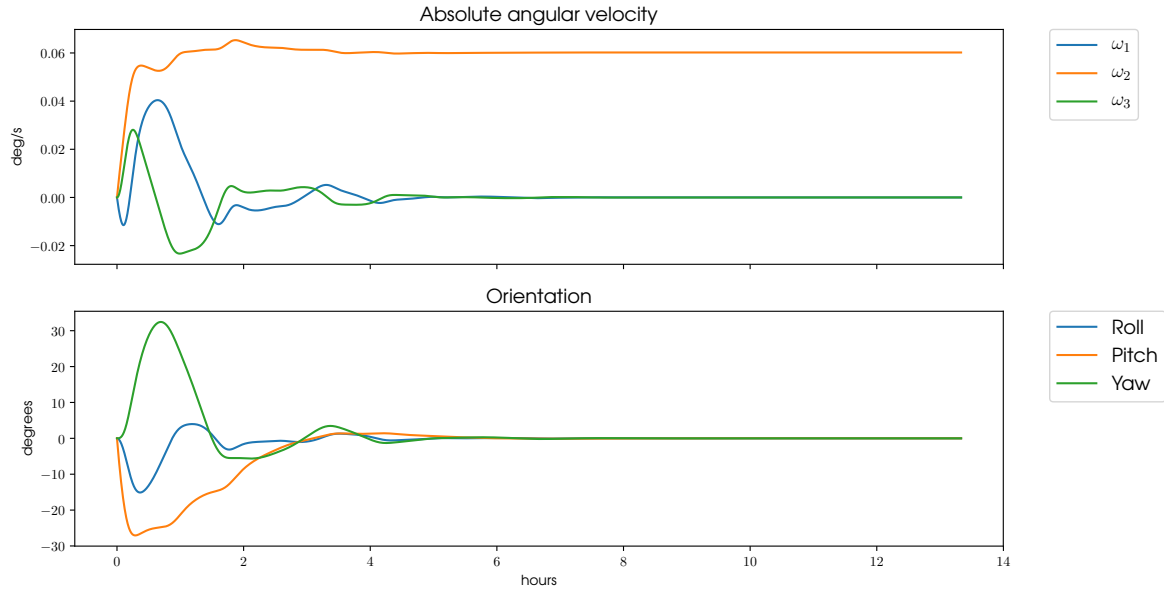


Figure 3: Absolute angular velocity ω^q and Euler angles without disturbances in a single satellite scenario.

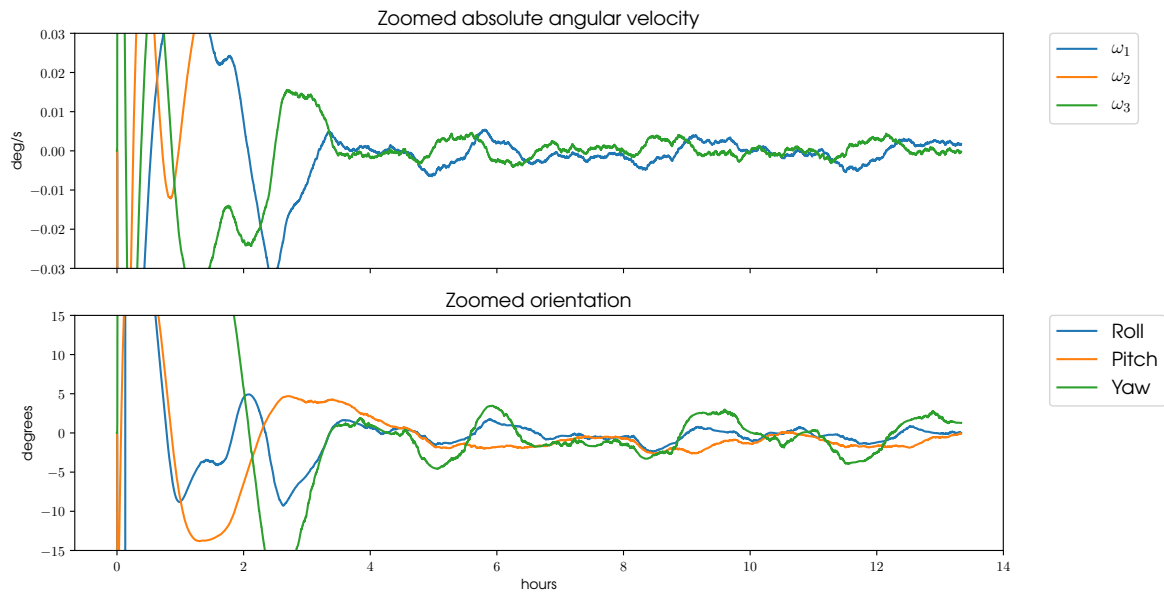


Figure 4: Absolute angular velocity ω^q and Euler angles with disturbances in a single satellite scenario.

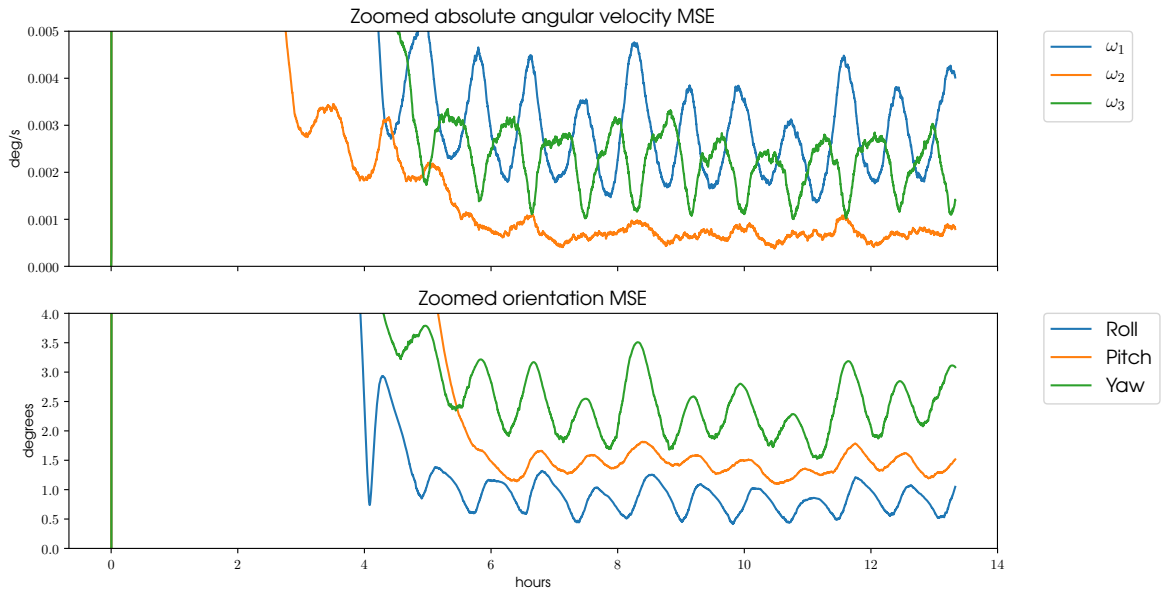


Figure 5: Mean-Squared Errors of the absolute angular velocity ω^q and Euler angles in a single satellite scenario.

SWARM SCENARIO

To enhance the accuracy of the attitude estimation we propose to take advantage of the fact that our mission is actually a swarm of CubeSats. The swarm comprises 4 spacecrafts, and their relative motion is further assumed to be such that they are constantly positioned in the vertices of a regular tetrahedron, which moves as a rigid body. The advantages of such a spatial configuration have been discussed in connection with various missions that had spatial or temporal environmental measurements as their primary objective.¹⁴ We shall not discuss here how such orbital motion can be implemented by the four spacecrafts, but refer the reader for the details to a study,¹⁵ where these matters are addressed.

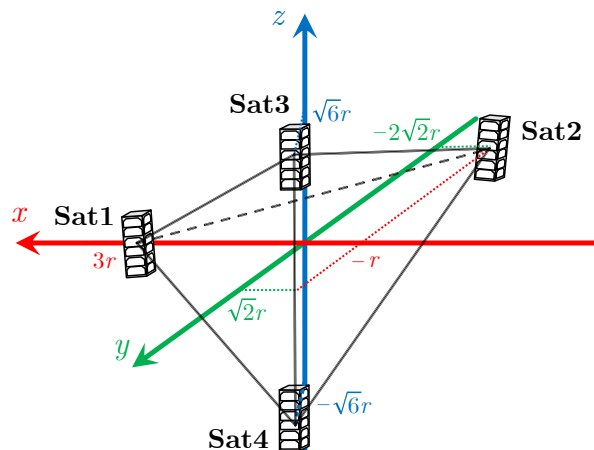


Figure 6: Swarm structure

The center of mass of the swarm is located in the center of tetrahedron and simultaneously on the same circular orbit, as it was in the single satellite scenario. It moves as a virtual 5th CubeSat, which collects the data on the attitude of all the swarm spacecraft. Since the data is concentrated in the center of mass, it makes sense to carry out calculations in the reference frame, bound to this point. Thus, the center of mass orbital frame is reintroduced – \mathcal{F}_0^u .

Position vectors of the swarm satellites in \mathcal{F}_0^u are defined as follows: $\mathbf{R}_0^{u_0}$ is the position vector of the center of mass, $\Delta\mathbf{R}_j^{u_0}$ is the position of the j^{th} satellite relative to the center of mass, $\mathbf{R}_j^{u_0} = \mathbf{R}_0^{u_0} + \Delta\mathbf{R}_j^{u_0}$ is the position vector of the j^{th} satellite.

$$\mathbf{R}_0^{u_0} = \begin{pmatrix} 0 \\ 0 \\ R_0 \end{pmatrix} \quad \Delta\mathbf{R}_j^{u_0} = \begin{pmatrix} \Delta x_j \\ \Delta y_j \\ \Delta z_j \end{pmatrix} \quad \mathbf{R}_j^{u_0} = \begin{pmatrix} \Delta x_j \\ \Delta y_j \\ R_0 + \Delta z_j \end{pmatrix} \quad (35)$$

Absolute values of vectors from Eq. (35) are identical in any frame and equal to $(R_0, \Delta R_j, R_j)$ respectively.

The tetrahedron used in the subsequent simulations is defined by its vertices (vectors $\Delta\mathbf{R}_j^{u_0}$) as:

$$\text{Sat1 } \Delta\mathbf{R}_1^{u_0} = (3r \ 0 \ 0)^\top$$

$$\text{Sat2 } \Delta\mathbf{R}_2^{u_0} = (-r \ -2\sqrt{2}r \ 0)^\top$$

$$\text{Sat3 } \Delta\mathbf{R}_3^{u_0} = (-r \ \sqrt{2}r \ \sqrt{6}r)^\top$$

$$\text{Sat4 } \Delta\mathbf{R}_4^{u_0} = (-r \ \sqrt{2}r \ -\sqrt{6}r)^\top$$

where r is the scaling coefficient. Hence, the size of tetrahedron is $2\sqrt{6}r$. The choice of vertices is illustrated in the figure 6. In the subsequent simulations the distances between any two vertices of the tetrahedral formation (i.e. edges of the tetrahedron) are assumed to be 50 km, which makes a formation of a reasonable size from the communication point of view.

Interpolation

The magnetic field is measured by the magnetometers of each satellite in the swarm. It means that we acquire these measurements (denoted as $\tilde{\mathbf{B}}_j^{q_j}$) in the body-fixed reference frame of the j^{th} satellite \mathcal{F}_j^q .

The obtained values are then converted to the respective orbital reference frame of the j^{th} satellite \mathcal{F}_j^u with the current quaternion Q_j :

$$\tilde{\mathbf{B}}_j^{u_j} = Q_j \circ \tilde{\mathbf{B}}_j^{q_j} \circ Q_j^* \quad (36)$$

After each satellite in the swarm has formed the values of magnetic field at its present location, the data must be sent over to the virtual CubeSat (hub) in the swarm's center of mass. To process the measurements data, the hub should convert all vectors to the single reference frame, which is center of mass orbital reference frame \mathcal{F}_0^u .

The conversion between \mathcal{F}_j^u and \mathcal{F}_0^u is carried out via DCM, which requires the position of the j^{th} satellite in \mathcal{F}_0^u . To fulfill this condition, each satellite, in addition, sends to the virtual CubeSat its position \mathbf{R}_j^{u0} to form the DCM $\mathbf{A}_{j \rightarrow 0}^u$. So, the measurements are converted:

$$\tilde{\mathbf{B}}_j^{u0} = \mathbf{A}_{j \rightarrow 0}^u \tilde{\mathbf{B}}_j^{uj} \quad (37)$$

Finally, the virtual hub estimates the value of the magnetic field in the center of mass \mathbf{B}_0^{u0} , using the interpolation methods with known tuples of (location, parameter) in the form $(\mathbf{R}_j^{u0}, \tilde{\mathbf{B}}_j^{u0})$. Our previous study⁸ employed Inverse Distance Weighting (IDW) to this end, however its obvious drawback is that it does not take into account spatial statistical properties of the geomagnetic field. To overcome this, the interpolation technique Kriging (described in the next section) is used as the best linear approximator.

Extrapolation

The interpolation procedure, as described in the previous section, takes place in the center of mass orbital reference frame \mathcal{F}_0^u . The output of the interpolation is the vector estimate of the geomagnetic field at the center of mass $\hat{\mathbf{B}}_0^{u0}$. Thus, having obtained the value of $\hat{\mathbf{B}}_0^{u0}$ we now need to determine the values of $\hat{\mathbf{B}}_j^{u0}$ (estimate of the magnetic field vector of j^{th} satellite in \mathcal{F}_0^u).

To do this, we need to find the function g , which returns the values of geomagnetic field at satellites' positions, given the value in the center of mass, the structure of the direct dipole model, and the location of each satellite \mathbf{R}_j^{u0} :

$$g : \mathbf{B}_0^{u0}, \mathbf{R}_j^{u0} \longrightarrow \mathbf{B}_j^{u0} \quad (38)$$

Let us write down expressions for \mathbf{B}_0^{u0} and \mathbf{B}_j^{u0} and compare them. \mathbf{B}_0^{u0} is straightforward Eq. (14), but for radius-vector \mathbf{R}_0^{u0} as in the single satellite scenario, because the center of mass is located on the orbit. Taking into account Eq. (14) it can be rewritten as:

$$\mathbf{B}_0^{u0} = -\frac{\mu_e \mu_0}{4\pi R_0^3} \begin{pmatrix} 1 & 0 & 0 \\ 0 & 1 & 0 \\ 0 & 0 & -2 \end{pmatrix} \mathbf{k}^{u0}, \quad \mathbf{k}^{u0} = -\begin{pmatrix} \cos u \sin i \\ \cos i \\ \sin u \sin i \end{pmatrix} \quad (39)$$

Expression for \mathbf{B}_j^{u0} is given by the dipole formula:

$$\mathbf{B}_j^{u0} = \frac{\mu_e \mu_0}{4\pi R_j^3} \left[\frac{3}{R_j^2} (\mathbf{k}^{u0} \cdot \mathbf{R}_j^{u0}) \mathbf{R}_j^{u0} - \mathbf{k}^{u0} \right] \quad (40)$$

It is clear that we can find vector \mathbf{k}^{u0} via Eq. (39) and substitute it into Eq. (40) to find \mathbf{B}_j^{u0} . Dipole vector \mathbf{k}^{u0} from Eq. (39):

$$\mathbf{k}^{u0} = -\frac{4\pi R_0^3}{\mu_e \mu_0} \begin{pmatrix} 1 & 0 & 0 \\ 0 & 1 & 0 \\ 0 & 0 & -\frac{1}{2} \end{pmatrix} \mathbf{B}_0^{u0} \quad (41)$$

Let us denote the matrix of coefficients from Eq. (41) as $\mathbf{I}_{-\frac{1}{2}}$. Then the substitution of Eq. (41) into Eq. (40), using new designation:

$$\mathbf{B}_j^{u_0} = \frac{R_0^3}{R_j^3} \left[\mathbf{I}_{-\frac{1}{2}} \mathbf{B}_0^{u_0} - \frac{3}{R_j^2} \left(\mathbf{I}_{-\frac{1}{2}} \mathbf{B}_0^{u_0} \cdot \mathbf{R}_j^{u_0} \right) \mathbf{R}_j^{u_0} \right] \quad (42)$$

Eq. (42) is the function g , defined in Eq. (38), which can be used to calculate estimates $\widehat{\mathbf{B}}_j^{u_0}$, based on the interpolated value $\widehat{\mathbf{B}}_0^{u_0}$:

$$\widehat{\mathbf{B}}_j^{u_0} = \frac{R_0^3}{R_j^3} \left[\mathbf{I}_{-\frac{1}{2}} \widehat{\mathbf{B}}_0^{u_0} - \frac{3}{R_j^2} \left(\mathbf{I}_{-\frac{1}{2}} \widehat{\mathbf{B}}_0^{u_0} \cdot \mathbf{R}_j^{u_0} \right) \mathbf{R}_j^{u_0} \right] \quad (43)$$

After we have got the estimates for magnetic field values $\widehat{\mathbf{B}}_j^{u_0}$ in the center of mass orbital reference frame \mathcal{F}_0^u , those values can be transformed into satellites' own orbital reference frame \mathcal{F}_j^u :

$$\widehat{\mathbf{B}}_j^{u_j} = \mathbf{A}_{0 \rightarrow j}^u \widehat{\mathbf{B}}_j^{u_0} \quad (44)$$

where $\mathbf{A}_{0 \rightarrow j}^u$ is the DCM of transition $\mathcal{F}_0^u \rightarrow \mathcal{F}_j^u$.

Enhanced values of the magnetic field vectors, which go into the observation model from Eq. (31) of each satellite, bounding orbital reference frame \mathcal{F}_j^u with body-fixed frame \mathcal{F}_j^q as in Eq. (36), are given by extrapolated estimates in Eq. (44).

KRIGING

Model

Kriging algorithms are a family of linear regression methods to estimate point values at any location within a given region.¹⁶ Unlike IDW and splines, which use predetermined analytical formulae defining the smoothness of the resulting curve and dependent only on the measurements of point values in the vicinity of the interpolated location, Kriging is based on the statistical models. The latter include autocorrelation analysis (relations between measured points). As a result, Kriging not only constructs predicted values surface, but also provides representation of the reliability or accuracy of such values.

Kriging takes into account spatial correlation between the data points, which is determined by the vector distances between them.

The point in the region is denoted by \mathbf{R} , and the value of the parameter measured at this point is denoted by $\widetilde{\mathbf{B}}(\mathbf{R})$ (since we measure the magnetic field¹⁷).

The estimator in Kriging is, as in IDW, weighted sum of measurements in the vicinity of the interpolated point:

$$\widehat{\mathbf{B}}(\mathbf{R}_0) = \sum_{j=1}^n \kappa_j \widetilde{\mathbf{B}}(\mathbf{R}_j) \quad (45)$$

where \mathbf{R}_0 is the interpolated point, $\widehat{\mathbf{B}}$ is the predicted value of the measured parameter, \mathbf{R}_j are the points available in the vicinity of interpolated one, κ_j are the weights, reflecting the spatial correlation between \mathbf{R}_j and \mathbf{R}_0 , n is the number of available points.

The measured function $\tilde{\mathbf{B}}(\mathbf{R})$ is assumed to be stationary, which implies the translation-invariance of the mean \mathbf{b}

$$\forall \mathbf{R} : \quad \mathbb{E} \left[\tilde{\mathbf{B}}(\mathbf{R}) \right] = \mathbf{b} \quad (46)$$

and the covariance $C(h)$ (for Ordinary Kriging (OK) only the distance is important, for different approaches in Kriging the direction between points can be used):

$$\begin{aligned} \forall \mathbf{R}_i, \mathbf{R}_j : \quad & |\mathbf{R}_i - \mathbf{R}_j| = h \\ \text{cov} \left(\tilde{\mathbf{B}}(\mathbf{R}_i), \tilde{\mathbf{B}}(\mathbf{R}_j) \right) &= C(\mathbf{R}_i - \mathbf{R}_j) \stackrel{\text{OK}}{=} C(h) \end{aligned} \quad (47)$$

where h is the distance between points, $C(h)$ is the translation-invariant function of covariance.

Variance minimization

The estimator $\hat{\mathbf{B}}(\mathbf{R}_0)$ should be unbiased (equal to the mean from Eq. (46)), which is achieved by setting the 1-norm of coefficients vector $\boldsymbol{\kappa}$ from Eq. (45) equal to 1:

$$\mathbb{E} \left[\hat{\mathbf{B}}(\mathbf{R}_0) \right] = \mathbb{E} \left[\tilde{\mathbf{B}}(\mathbf{R}_0) \right] = \mathbf{b} \quad \iff \quad \sum_{i=1}^n \kappa_i = 1 \quad (48)$$

Then we can minimize the variance of the estimator prediction σ_e^2 , using unbiasedness in Eq. (48):

$$\sigma_e^2 = \text{D} \left[\hat{\mathbf{B}}(\mathbf{R}_0) - \tilde{\mathbf{B}}(\mathbf{R}_0) \right] = \mathbb{E} \left[\hat{\mathbf{B}}(\mathbf{R}_0) - \tilde{\mathbf{B}}(\mathbf{R}_0) \right]^2 \quad (49)$$

where D is variance.

Expanding Eq. (49) in terms of Eq. (47):

$$\sigma_e^2 = \sigma^2 + \sum_{i=1}^n \sum_{j=1}^n \kappa_i \kappa_j C(\mathbf{R}_i - \mathbf{R}_j) - 2 \sum_{i=1}^n \kappa_i C(\mathbf{R}_i - \mathbf{R}_0) \quad (50)$$

where $\sigma^2 = \text{D} \left[\tilde{\mathbf{B}}(\mathbf{R}_i) \right] = C(0)$ – variance of measured point.

Thus, we are facing a minimization problem with objective function from Eq. (50) and constraint in the form of unbiasedness in Eq. (48):

$$\min_{\boldsymbol{\kappa}} \sigma_e^2 \quad \text{w.r.t.} \quad \sum_{i=1}^n \kappa_i = 1 \quad (51)$$

The problem from Eq. (51) can be solved via dual problem with Lagrange multiplier $2\boldsymbol{\varkappa}$, assigned to constraint from Eq. (48). The Lagrangian \mathcal{L} will have the form:

$$\mathcal{L} = \sigma_e^2 - 2\boldsymbol{\varkappa} \left(\sum_{i=1}^n \kappa_i - 1 \right) \quad (52)$$

Necessary condition of the minimum:

$$\begin{cases} \frac{1}{2} \frac{\partial \mathcal{L}}{\partial \kappa_i} = \sum_{j=1}^n \kappa_j C(\mathbf{R}_i - \mathbf{R}_j) - C(\mathbf{R}_i - \mathbf{R}_0) - \boldsymbol{\varkappa} = 0, \\ \frac{1}{2} \frac{\partial \mathcal{L}}{\partial \boldsymbol{\varkappa}} = \sum_{j=1}^n \kappa_j - 1 = 0, \end{cases} \quad (53)$$

which is a system of equations for the vector $\boldsymbol{\kappa}$ and the multiplier \varkappa via covariances $C(h)$.

Usually instead of covariances $C(h)$ in system of equations (53) semivariances $\gamma(h)$ are used. The semivariance is one half of the variance between adjacent measurements and has the following connection with covariance (semivariances are also translation-invariant):

$$\gamma(\mathbf{R}_i - \mathbf{R}_j) = \frac{1}{2} \text{D} \left[\tilde{\mathbf{B}}(\mathbf{R}_i) - \tilde{\mathbf{B}}(\mathbf{R}_j) \right] = \sigma^2 - C(\mathbf{R}_i - \mathbf{R}_j). \quad (54)$$

Now, let us rewrite system (53) in terms of semivariances from Eq. (54):

$$\begin{cases} \sum_{j=1}^n \kappa_j \gamma(\mathbf{R}_i - \mathbf{R}_j) + \varkappa = \gamma(\mathbf{R}_i - \mathbf{R}_0), \\ \sum_{j=1}^n \kappa_j = 1. \end{cases} \quad (55)$$

Semivariograms

System (55) yields vector $\boldsymbol{\kappa}$ as the output, to calculate the estimator from Eq. (45), however in order to solve it we need a priori information about the semivariances $\gamma(h)$.

To collect the information about the semivariance of the measured parameter in the given region, the empirical semivariogram is built. Empirical semivariogram is a non-parametric function, which accepts the distance between measured points h as an argument and returns the approximate semivariance for points located at a distance h from each other:

$$\begin{aligned} \forall \mathbf{R}_i, \mathbf{R}_j : \quad |\mathbf{R}_i - \mathbf{R}_j| = h \\ \gamma(h) = \frac{1}{2n_h} \sum_{(i,j)=1}^{n_h} \left(\tilde{\mathbf{B}}(\mathbf{R}_i) - \tilde{\mathbf{B}}(\mathbf{R}_j) \right)^2, \end{aligned} \quad (56)$$

where n_h is the total number of sampled points pairs.

Having amassed enough data in the empirical semivariogram, we can approximate it with some model function, which ensures validity. This is necessary, due to discontinuity of functions in Eq. (56).

Model functions usually have the following parameters:

- nugget – measure of discontinuity at the origin,
- sill – $\lim_{h \rightarrow \infty} \gamma(h)$,
- range – distance h , at which $\gamma(h) = 0.95$ sill.

These parameters are illustrated on the figure 7. There is a vast majority of such models, but for brevity we will use only one of the most common ones – powered exponential:

$$\gamma(h) = \begin{cases} c_0 + c \left(1 - \exp \left[- \left(\frac{h}{a} \right)^\nu \right] \right), & h > 0 \\ 0, & h = 0 \end{cases} \quad (57)$$

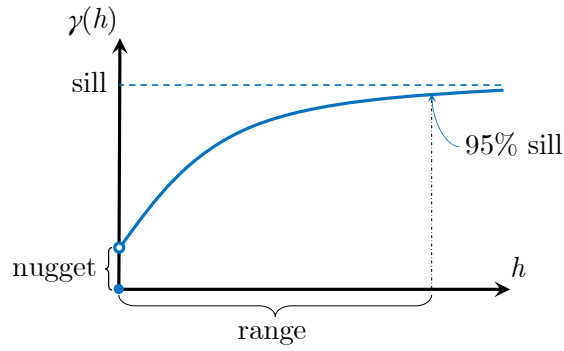


Figure 7: Semivariogram model function parameters

where c_0 is the nugget, $c_0 + c$ is the sill, range is approximately $3a$, and ν is the power of the exponent. If $\nu = 1$ the model is called exponential, and if $\nu = 2$ it is called gaussian.

Since we use direct dipole model of the magnetic field, we can create the empirical semivariogram on the observations, which fit this model.

In the figure 8 empirical semivariogram is plotted with power exponential model function. As the result, the semivariogram from Eq. (57) to be used for swarm scenario filtering has the following parameter values: $c_0 = 0.02 \mu\text{T}^2$, $c = 1.5 \mu\text{T}^2$, $a = 127 \text{ km}$, $\nu = \frac{8}{3}$.

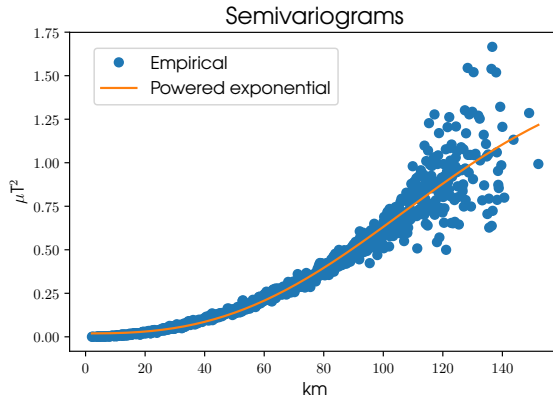


Figure 8: Semivariogram of the direct dipole magnetic field on the circular orbit with altitude $h_{\text{orb}} = 750 \text{ km}$ and inclination $i = 60^\circ$. $n = 2000$ points is taken in the vicinity of the point on orbit with argument of latitude $u = 60^\circ$ ($n_h = 19900$ averaged to 1000). The vicinity is defined as the cube with center in the point of the orbit and sides, equal to 50 km

Results and Discussion

Simulation results of filtering with Kriging are presented in the figure 9. Plots are given only for 1 satellite out of 4, because the results a similar. Parameters of the orbit, CubeSats, controller and noises are the same as in the single satellite scenario. In comparison with the figure 5 the accuracy of the orientation in the current plot is one degree better, which is the best case in simulations. It shows that the Ordinary Kriging interpolation does ensure a noticeable attitude control enhancement.

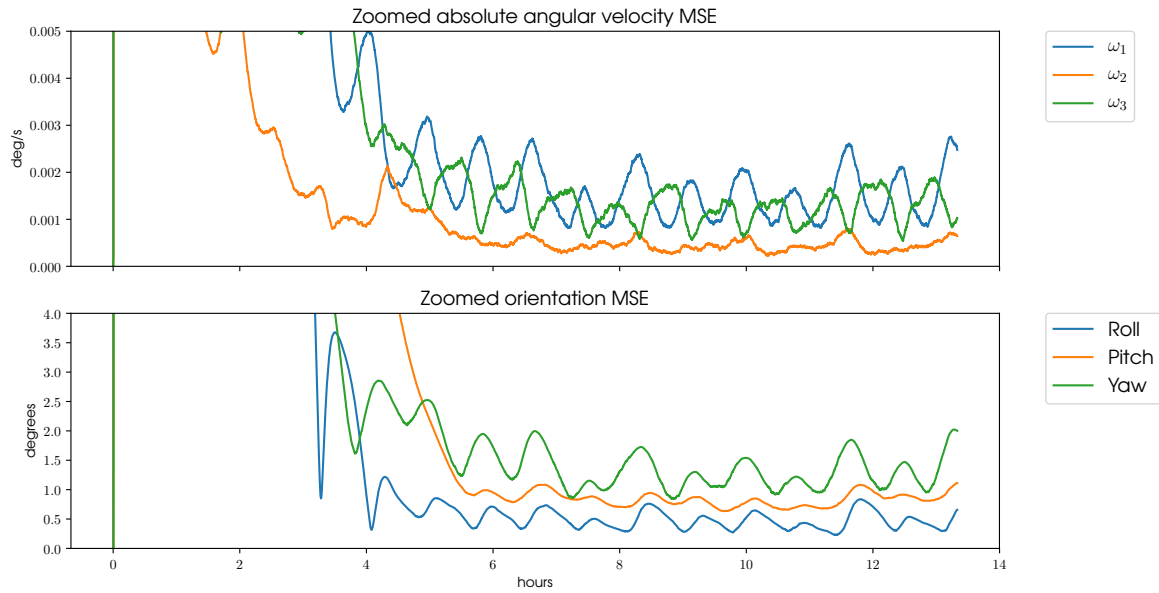


Figure 9: Mean-Squared Errors of the absolute angular velocity ω^q and Euler angles in a swarm scenario

Our simulation results indicate that the attitude determination and control system of a swarm may indeed become more robust than that of a single satellite. However, there remains a number of open questions, which shall be addressed in the future research:

1. In this study the powered exponential model function is used, since it was a best fit for the empirical semivariogram obtained for the direct dipole magnetic field model. Which semi-variogram model should be used to enhance attitude accuracy?
2. Currently, the region of interpolated points is defined by the size of swarm tetrahedron (equals to its edge). What is the actual range of Kriging? And at what point observations become unreliable?
3. The swarm moves as a rigid body and conserves its distances throughout the whole period on the orbit. How the attitude MSEs will change when the relative movement around the swarm's center of mass will be implemented?
4. The Ordinary Kriging is used — when correlation weights in semivariogram are dependant only on the absolute value of the lag distance h . How will the accuracy change, if the Kriging with trends (directions of \mathbf{h}) will be used? Is it excessive to implement temporal Kriging?
5. The empirical semivariogram is obtained using the dependence of the semivariance between a couple of points and the Euclidean distance between them. Will semivariogram be more precise, if the spherical distance or another dependent parameter is used?
6. Currently, there are only 4 CubeSats in the swarm. How the orientation accuracy changes with the number of satellites involved? Is the dependency monotonic or there is a saturation point?

7. Direct dipole is an oversimplified model of the measurement field, which makes spatial correlation more robust than it really is. How will the usage of the IGRF-12 affect empirical semivariogram precision?

CONCLUSION

Our study delineates a method to enhance attitude determination algorithms in a satellite swarm by exchanging and processing distributed measurements of the geomagnetic field. Kriging interpolator has been implemented to simulate the communication between the swarm nodes and enhance the attitude control on the basis of optimized magnetic field measurements. To analyze the spatial correlation in the interpolation region, an empirical semivariogram, based on the direct dipole of the geomagnetic field, is acquired and fit into the powered exponential mathematical model, which was used in the communication algorithm. Based on the proposed determination algorithm, a complete set of solely magnetic attitude control algorithms is developed, implemented and tested by numerical experiments. Filtration of CubeSat's magnetic ADCS is performed and compared with the filtration in the swarm. It appears that the the system which uses the interpolator has on average 0.5° better accuracy. However, the disturbances used in simulations are rather small and the in-orbit resulting MSEs are expected to be different, with greater standard deviations and non-zero means.

To sum up, CubeSats' orientation enhancement via decentralized communication and magnetic field interpolation has been tested in the simple scenario, and found to be working as intended. However, there is still a lot of questions, listed in the results subsection, which should be addressed to improve the robustness of the algorithm in the real life missions.

ACKNOWLEDGMENT

This work is funded by RFBR, project number 19-38-90278.

REFERENCES

- [1] D. Selva, A. Golkar, O. Korobova, I. L. i. Cruz, P. Collopy, and O. De Weck, "Distributed earth satellite systems: What is needed to move forward?," *Journal of Aerospace Information Systems*, Vol. 14, No. 8, 2017, pp. 412–438.
- [2] C. Araguz, E. Bou-Balust, and E. Alarcón, "Applying autonomy to distributed satellite systems: Trends, challenges, and future prospects," *Systems Engineering*, Vol. 21, No. 5, 2018, pp. 401–416, 10.1002/sys.21428.
- [3] S. Lem, *Summa Technologiae*. Suite 290 111 Third Avenue South, Minneapolis: Univ Of Minnesota Press, 1st ed., 2013.
- [4] A. Farrag, T. Mahmoud, and A. Y. ELRaffiei, "Satellite swarm survey and new conceptual design for Earth observation applications," *The Egyptian Journal of Remote Sensing and Space Science*, 2019, <https://doi.org/10.1016/j.ejrs.2019.12.003>.
- [5] F. Fiore, L. Burderi, T. D. Salvo, M. Feroci, C. Labanti, M. R. Lavagna, and S. Pirrotta, "HERMES: a swarm of nano-satellites for high energy astrophysics and fundamental physics," *Space Telescopes and Instrumentation 2018: Ultraviolet to Gamma Ray* (J.-W. A. d. Herder, S. Nikzad, and K. Nakazawa, eds.), Vol. 10699, International Society for Optics and Photonics, SPIE, 2018.
- [6] A. Annenkova, S. Biktimirov, K. Latyshev, A. Mahfouz, P. Mukhachev, and D. Pritykin, "Cubesat ADCS model for preliminary design procedures within a concurrent design approach," *AIP Conference Proceedings*, Vol. 2171, No. 140005, 2019.
- [7] Y. Menshenin, K. Latyshev, A. Mahfouz, and D. Pritykin, "Applying the model-based conceptual design approach to ADCS development: A case study of a CubeSat swarm mission," *Proceedings of the International Astronautical Congress, IAC*, Vol. 2019-October, No. IAC-19.D1.2.8_x50723, 2019.
- [8] A. Mahfouz, D. Pritykin, A. Afanasev, A. Annenkova, and K. Latyshev, "Coordinated attitude determination and control in a swarm of CubeSats," *Proceedings of the International Astronautical Congress, IAC*, Vol. 2019-October, No. IAC-19.C1.6.9_x52687, 2019.

- [9] D. Ivanov, M. Ovchinnikov, V. Penkov, D. Roldugin, D. Doronin, and A. Ovchinnikov, "Advanced numerical study of the three-axis magnetic attitude control and determination with uncertainties," *Acta Astronautica*, Vol. 132, 2017, pp. 103–110.
- [10] M. Desouky, K. Prabhu, and O. Abdelkhalik, "On spacecraft magnetic attitude control," *Space Flight Mechanics Meeting, 2018*, No. 210009, 2018.
- [11] M. Ovchinnikov, D. Roldugin, D. Ivanov, and V. Penkov, "Choosing control parameters for three axis magnetic stabilization in orbital frame," *Acta Astronautica*, Vol. 116, 2015, pp. 74–77.
- [12] R.E. Kalman, R.S. Bucy, "New results in linear filtering and prediction theory," *Trans. ASME, Ser. D. J. Basic Eng.*, Vol. 83, 1961, pp. 95–108.
- [13] D. Ivanov, M. Ovchinnikov, N. Ivlev, and S. Karpenko, "Analytical study of microsatellite attitude determination algorithms," *Acta Astronautica*, Vol. 116, 2015, pp. 339–348.
- [14] J. J. Guzman and A. Edery, "Mission design for the MMS tetrahedron formation," *2004 IEEE Aerospace Conference Proceedings (IEEE Cat. No.04TH8720)*, Vol. 1, March 2004, p. 540 Vol.1.
- [15] S. Shestakov, M. Ovchinnikov, and Y. Mashtakov, "Analytical Approach to Construction of Tetrahedral Satellite Formation," *Journal of Guidance, Control, and Dynamics*, Vol. 42, No. 12, 2019, pp. 2600–2614.
- [16] T.C. Bailey, A.C. Gatrell, *Interactive Spatial Data Analysis*. Informa PLC, 5 Howick Place, London: Routledge, 1st ed., 1995.
- [17] K. M. Campbell, "Comparing Accuracies of Spatial Interpolation Methods on 1-Minute Ground Magnetometer Readings," Master's thesis, North Dakota State University, North Dakota, 2017.